

Article

Optimization of Pitch Control Parameters for a Wind Turbine Based on Tower Active Damping Control

Yingming Liu ^{1,*}, Shuyuan Zhang ^{1,*}, Xiaodong Wang ¹, Hongfang Xie ² and Tian Cao ^{3,*}

¹ School of Electrical Engineering, Shenyang University of Technology, Liao Shen West Road 111, Shenyang 110027, China

² School of Electric Power, Shenyang Institute of Technology, Pu Chang Road 18, Shenyang 110136, China

³ School of Electrical Engineering, China University of Mining and Technology, University Road 1, Xuzhou 221116, China

* Correspondence: z572280373@163.com (S.Z.); caotcumt@126.com (T.C.)

Abstract: Given the difficulty of accurately setting multiple control parameters in wind turbines, a design method for a pitch controller considering tower load reduction is proposed, which enhances the control performance and reduces both the tower vibration and load. Firstly, the pitch-speed system and the tower fore-aft active damping control are built. In addition, the explicit equation of the tower fore-aft active damping gain is deduced to calculate its initial value. Secondly, the pitch-speed system is identified as an inertial time-delay system using the least squares method. Subsequently, the pitch PI control parameters are set using the Chien–Hrones–Reswick method. Thirdly, the pitch PI control parameters and the tower fore-aft active damping gains are optimized based on the kindred-protected genetic algorithm, which improves the accuracy of the control parameters. Meanwhile, the Pareto method is used to coordinate the control objectives by allocating the weight. Furthermore, the adaptive control is built by fitting the parameters with the wind speed points using the least squares method to enhance the control performance. Finally, the effectiveness of the proposed design method is verified by comparing the control performance with the tower vibration and load.

Keywords: wind turbine; pitch-speed system; PI; damping; optimization strategy



Citation: Liu, Y.; Zhang, S.; Wang, X.; Xie, H.; Cao, T. Optimization of Pitch Control Parameters for a Wind Turbine Based on Tower Active Damping Control. *Energies* **2022**, *15*, 8686. <https://doi.org/10.3390/en15228686>

Academic Editors: Yolanda Vidal and Davide Astolfi

Received: 27 September 2022

Accepted: 16 November 2022

Published: 18 November 2022

Publisher's Note: MDPI stays neutral with regard to jurisdictional claims in published maps and institutional affiliations.



Copyright: © 2022 by the authors. Licensee MDPI, Basel, Switzerland. This article is an open access article distributed under the terms and conditions of the Creative Commons Attribution (CC BY) license (<https://creativecommons.org/licenses/by/4.0/>).

1. Introduction

At present, the mature pitch control is extensively adopted in wind turbines. Therefore, the research on pitch PI control holds great theoretical significance and engineering prospects. The pitch angle is adjusted by the pitch PI control in wind turbines to operate the wind turbine at the rated power [1,2]. However, during pitch control, wind loads can cause fore-aft vibration in the tower. It is necessary to provide the additional pitch angle through the fore-aft active damping control to restrain the tower fore-aft vibration [3,4]. In addition, the problem of the inaccurate setting of control parameters caused by the mutual coupling of multiple control parameters requires an urgent solution [5]. At the same time, it is worthwhile to research how to coordinate the two control objectives of enhancing control performance and reducing the load situation of the tower [6]. In summary, a design method for a pitch controller considering tower load reduction deserves in-depth research.

Currently, researchers are studying the design of pitch controllers. First of all, many researchers have proposed different identification methods for various systems according to frequency or time domain characteristic. In reference [7], the large delay characteristic is ignored, which will seriously impact the identification accuracy. Therefore, there will be an impact on the subsequent optimization of the control parameters. Next, the PI controller is generally designed according to the input and output results of the step response [8]. However, in simulation or engineering, the input to the PI controller is not a simple step signal, but a complex continuously changing motion. Therefore, the PI controller designed according to the step response is not sufficiently adaptable to complex operating conditions.

In recent years, there has been a broad focus on reducing the tower load by increasing the damping. In reference [9], the PI controller and active damping controller are designed separately. The comprehensive performance of the two controllers designed separately is not necessarily optimal because the mutually influencing factors are neglected. Therefore, both controllers need to be designed simultaneously to achieve the optimal comprehensive control effect. Furthermore, intelligent algorithms with universal applicability are widely adopted to optimize control parameters. In reference [10], only a single type of turbulent wind condition is considered as a system input when the intelligent algorithm is used. However, the wind turbine operating state varies with wind conditions, and the effects of different wind types and turbulence intensities need to be considered. Comparative tests must be designed to verify under which turbulent wind conditions the intelligent algorithm is better optimized. In reference [11], the authors suggest that a genetic algorithm (GA) can be adopted to optimize the PID control parameters of the inverter motor speed governing system. However, the poor population diversity of GA leads to an insufficient global search capability, thus falling into the local optimum. Therefore, the effect of optimizing the control parameters based on the GA cannot always achieve optimal results. In reference [12], particle swarm optimization (PSO) is adopted to optimize the PID control parameters; however, its poor convergence leads to insufficient local search capability. Therefore, it will take a long time for the PSO algorithm to optimize the control parameters. In reference [13], only the single control objective of reducing the fluctuations in regards to power and generator speed are considered for the designed pitch controller, without considering the tower load of the wind turbine. Determining a method for reducing the tower load of wind turbines based on the enhanced control performance deserves in-depth research. Therefore, the method of coordinating control objectives has become a research hotspot. In reference [14], the weight is allocated by orthogonal experiments. However, it required a large number of experiments to determine the effect of each group of PI controllers on the individual pitch control and the performance index function. In addition, since constant PI control parameters cannot always maintain excellent control performance, adaptive control has received more and more attention from scholars. In reference [15], the gain scheduling controller is designed in conjunction with the wind speed. However, including the gain factor in gain scheduling increases the complexity of the controller.

In order to solve the above problems, a design method for a pitch controller, considering tower load reduction, is proposed. An explicit equation for tower fore-aft active damping gain is deduced. In addition, the pitch-speed system, with a large time delay characteristic, is identified as an inertial time-delay system. Moreover, in the kindred-protected genetic algorithm (KPGA), the effects of different turbulent wind types and turbulence intensities on the optimization results are considered as system inputs, and the pitch system PI control parameters and tower fore-aft active damping gain are optimized simultaneously. At the same time, the Pareto method is used to coordinate the control objectives by allocating weight. In summary, the main contributions are as follows.

- (1) The pitch-speed system is identified as an inertial time-delay system, which can accurately reflect the large time delay characteristic of the pitch-speed system and solve the problem of its poor identification accuracy, thereby facilitating the obtaining of optimal control parameters.
- (2) An explicit equation of tower fore-aft active damping gain is deduced, in detail. This explicit equation can solve the problem of the difficulty of determining the active damping gain of the tower fore-aft, providing a more convenient and accurate calculation method to reduce the tower vibration and load by using active damping control.
- (3) Considering the effects of different turbulent wind types and turbulence intensities, a KPGA optimization method is proposed to overcome the risk of falling into the local optimum by increasing population diversity, thereby obtaining more accurate control parameters. Meanwhile, the weight is allocated by the Pareto method to coordinate control objectives, which can reduce load situations while enhancing control performance.

In Section 2, the pitch-speed system and tower fore-aft active damping controllers are built. In addition, the explicit equation of the tower fore-aft active damping gain is deduced to calculate its initial value. In Section 3, the pitch-speed system is identified as an inertial time-delay system using the least squares method. Subsequently, the pitch system PI control parameters are set using the Chien–Hrones–Reswick method. In Section 4, an optimization method of KPGA is proposed to optimize the control parameters. Furthermore, an adaptive control is built using the least squares method. In Section 5, the results of the simulation verification are presented. In Section 6, the conclusions are summarized, and future research directions are planned.

2. Mathematical Model and Dynamic Model

In traditional pitch control, the generator speed difference $\Delta\omega$ is used as an input to the pitch PI controller. The value of $\Delta\omega$ is calculated from the measured value $\omega_{measure}$ and the rated value ω_{rated} . The rated pitch angle is used as an output to the pitch PI control. Since the first-order modal fore-aft damping of the tower is small, fore-aft vibration easily occurs under the influence of wind load. Therefore, the tower fore-aft active damping control is added to increase the equivalent damping, thus restraining the fore-aft tower vibration. Since the velocity at the top of the tower \dot{x} is difficult to measure, it is usually chosen to measure the acceleration \ddot{x} to obtain the velocity. Subsequently, the additional pitch angle $\Delta\beta_2$ is obtained by multiplying the velocity of the tower top by the active damping gain K_a . Thereby, the rated pitch angle β_1 , provided by the traditional pitch control, and $\Delta\beta_2$, provided by the tower fore-aft active damping control, constitute the given pitch angle β of the pitch-speed system. Therefore, the principle of novel pitch control is shown in Figure 1.

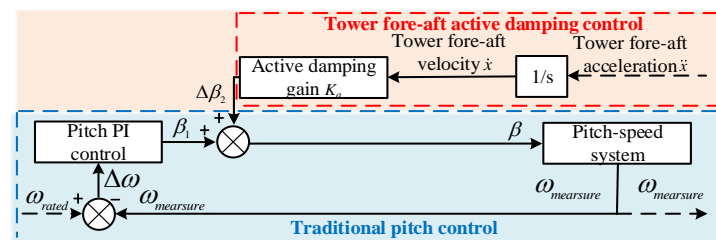


Figure 1. The principle of novel pitch control.

The physical model of the 2 MW wind turbine is provided by Bladed software. Bladed software has been certified by Germanischer Lloyd (GL) and the International Electrotechnical Commission (IEC) and is broadly recognized by researchers. The main parameters of the 2 MW wind turbine are as follows: a wind turbine operating range 4~25 m/s, a rated generator speed 1500 r/min, a pitch range 0~90°, a rated pitch angle 0°, a pitch control range of 12~25 m/s, and a first-order modal natural frequency fore-aft of the tower of 2.95 rad/s.

2.1. Pitch-Speed System Mathematical Model

Since the pitch PI control parameters need to be set, the wind turbine physical model must be converted to the pitch-speed system mathematical model. The Taylor series expansion can be used to linearize the nonlinear wind turbine into a state-space equation. Then the pitch-speed system mathematical model can be obtained by further extracting variables from the state-space equation.

Since a wind turbine is a nonlinear system, the physical model of the 2MW wind turbine, provided by the Bladed software, is a nonlinear wind turbine. Therefore, it is converted to a linear model using the Taylor series expansion in the Bladed software. The principle of the Taylor series expansion is shown in Equation (1).

$$y = f(x_0) + \left. \frac{df(x)}{dx} \right|_{x=x_0} (x - x_0) + \frac{1}{2!} \left. \frac{d^2f(x)}{dx^2} \right|_{x=x_0} (x - x_0)^2 + \dots \quad (1)$$

where, x_0 denotes each balance point.

The balance points are the wind speed points with a step size of 1 in the operating range of the wind turbine. Since this paper only studies the pitch control of the wind turbines, only the balance points within the pitch control range are researched. Therefore, the rest of the wind speed points with a step size of 0.1 are considered to be located away from the balance points in pitch control range.

According to the Taylor series expansion for each balance point, a complex state space equation is obtained by linearizing the nonlinear wind turbine [16,17], which is shown in Equation (2).

$$\begin{cases} \dot{x} = Ax + Bu \\ y = Cx + Du \end{cases} \quad (2)$$

where A , B , C , and D denote three-dimensional coefficient matrices. The third dimension is the balance point. x , u , and y denote the state variable, input variable, and output variable. Equation (2) is shown in detail in Appendix A.

A further extraction of variables from Equation (2) is required in order to obtain the pitch-speed system mathematical model. Therefore, an input, output, and wind speed point is extracted from Equation (2) in MATLAB to obtain a transfer function at a certain balance point [18,19]. The $G_{16}(s)$ denotes a pitch-speed system at a wind speed of 16 m/s, as shown in Equation (3).

$$G_{16}(s) = [0.00074079(s + 563)(s + 15.46)(s - 12.89)(s^2 - 0.04007s + 8.593)(s^2 + 0.1069s + 9.154)(s^2 + 1.353s + 112.6)(s^2 + 3.591s + 275.3)(s^2 + 9.724s + 378.4)(s^2 + 0.3071s + 544.4)(s^2 + 0.3738s + 745.3)(s^2 - 687.8s + 2.245 \times 10^6)] / [(s + 3.333)(s + 0.2115)(s^2 + 0.3566s + 8.858)(s^2 + 0.04065s + 8.881)(s^2 + 3.89s + 46.74)(s^2 + 1.963s + 191.9)(s^2 + 3.48s + 339.4)(s^2 + 5.646s + 467.1)(s^2 + 1.135s + 524.1)(s^2 + 2.32s + 638.9)(s^2 + 4.851s + 4162)] \quad (3)$$

According to the above method, the pitch-speed system in 12~25 m/s for the 2 MW wind turbine is established for each balance point in turn.

The pitch-speed system is built, and the tower fore-aft active damping control will be built subsequently.

2.2. Tower Fore-Aft Active Damping Control Dynamic Model

A tower, nacelle, and rotor form the basic structure of a wind turbine. Among these, the nacelle and the rotor can be equivalent to the particle P. Therefore, the typical cantilever beam model and simplified model are shown below.

According to the simplified model of wind turbines shown in Figure 2, the first-order dynamic response fore-aft of the tower can be expressed as the second-order damping resonance motion [20,21].

$$M_i \ddot{x}_i + D_i \dot{x}_i + K_i x_i = F_i + \Delta F_i \quad (4)$$

where, M_i denotes the modal mass of the tower, D_i denotes the modal damping, K_i denotes the modal rigidity, \ddot{x}_i denotes the tower top mode acceleration, \dot{x}_i denotes the tower top mode velocity, x_i denotes the tower top mode displacement, F_i denotes the axial force of the rotor, and ΔF_i denotes the additional force caused by the incentive change.

In these models, the ΔF_i can be defined as:

$$\Delta F_i = -B\dot{x}_i \quad (5)$$

where B denotes the additional damping provided by rotor aerodynamic damping.

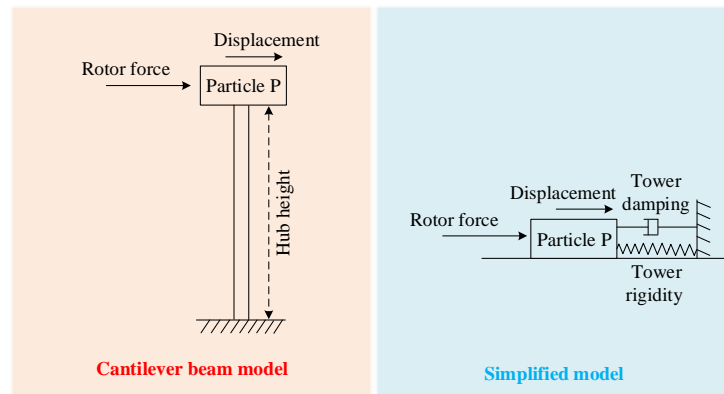


Figure 2. The typical cantilever beam model and the simplified model.

From Equations (4) and (5), it can be deduced:

$$M_i \ddot{x}_i + (D_i + B) \dot{x}_i + K_i x_i = F_i \tag{6}$$

According to the deduction of the above equation, the equivalent damping of the tower is enhanced from D_i to $(D_i + B)$.

Subsequently, the ΔF_i can be further expressed as:

$$\Delta F_i = -B \dot{x}_i = \frac{\partial F_i}{\partial \beta_i} \Delta \beta_i \tag{7}$$

According to Equation (7), it can be deduced that the relationship between the additional pitch angle and the tower top fore-aft velocity is as follows.

$$\Delta \beta_i = \frac{-B}{\partial F_i / \partial \beta_i} \dot{x}_i = K_a \dot{x}_i \tag{8}$$

where $\partial F_i / \partial \beta_i$ denotes the force and pitch angle curve and K_a denotes the active damping gain.

According to Equation (8), aerodynamic damping B is required to calculate the active damping gain. Therefore, a linear relationship between load fluctuation q and wind speed fluctuation u acting on the blade of unit length can be expressed as:

$$q = \frac{1}{2} \rho \Omega r c(r) \frac{dC_L}{d\alpha} u \tag{9}$$

where ρ denotes air density, Ω denotes the rotor speed, $C(r)$ denotes the airfoil chord at the radius r of the rotor, and $dC_L / d\alpha$ denotes the change rate of a lift coefficient C_L to an angle of attack α .

Moreover, the wind speed fluctuation u can be replaced with blade waving speed $-\dot{x}_h$. Then, the aerodynamic damping \dot{B} of the blade per unit length can be expressed as:

$$\dot{B} = \frac{q}{-\dot{x}_h} = \frac{1}{2} \rho \Omega r c(r) \frac{dC_L}{d\alpha} \tag{10}$$

Subsequently, the aerodynamic damping B of the rotor can be expressed as:

$$B = A \int \dot{B} dr = \frac{1}{2} A \rho \Omega \frac{dC_L}{d\alpha} \int_0^R r c(r) dr \tag{11}$$

where A denotes the number of the wind turbine blades.

Therefore, the explicit equation of the active damping gain can be expressed as:

$$K_a = \frac{-B}{\partial F_i / \partial \beta_i} = \frac{\frac{1}{2} A \rho \Omega \frac{dC_L}{d\alpha} \int_0^R rc(r) dr}{\partial F_i / \partial \beta_i} \quad (12)$$

The parameters are provided by the Bladed software. Therefore, the tower active damping gain initial value K_a can be obtained by Equation (12).

3. System Identification and Parameters Setting

3.1. Pitch-Speed System Identification

Since the pitch-speed system $G_{16}(s)$ exhibits the characteristics of large inertia and large time delay, the transfer function method and the least squares method are adopted to identify it as an inertial time-delay system. The basic form of the inertial time-delay system can be expressed as:

$$G(s) = \frac{K}{Ts + 1} e^{-Ls} \quad (13)$$

where K denotes the final value, L denotes the delay, and T denotes the rise time.

The principle of the transfer function method is shown below [22]. Find the first-order derivative and second-order derivative of $G(s)$ with respect to s , and it can be deduced.

$$\frac{G'(s)}{G(s)} = -L - \frac{T}{1 + Ts} \quad (14)$$

$$\frac{G''(s)}{G(s)} - \left(\frac{G'(s)}{G(s)}\right)^2 = \frac{T^2}{(1 + Ts)^2} \quad (15)$$

Find the value of each order derivative at $s = 0$.

$$T_{ar} = -\frac{G'(0)}{G(0)} = L + T \quad (16)$$

$$T^2 = \frac{G''(0)}{G(0)} - T_{ar}^2 \quad (17)$$

where T_{ar} denotes the average residence time.

By the above derivation, the equation of L is calculated as $L = T_{ar} - T$. K can be obtained from $G(0)$. The above transfer function method can identify the pitch-speed system as an inertial time-delay system.

Since the stability and identification accuracy of the least squares method can meet the requirements, it is suitable for identifying complex models [23]. The basic principle of the least squares method is shown in Equation (18).

$$z(k) = h^T(k)\theta + e(k) \quad (18)$$

where $z(k)$ denotes the k -th output measurement, h denotes a sample set, θ denotes a set of parameters to be identified, and $e(k)$ denotes random noise.

Furthermore, the least squares method performance index is shown in Equation (19).

$$J(\theta) = \sum_{k=1}^{\infty} [z(k) - h^T(k)\theta]^2 \quad (19)$$

Therefore, the inertial time-delay system is identified by the least squares method when the cumulative sum of the squared deviations calculated according to Equation (19) reaches a minimum value.

Based on the transfer function and least squares methods, Equation (3) is respectively identified as inertial time-delay systems $G_{16_tf}(s)$ and $G_{16_least}(s)$, as is shown in Equations (20) and (21).

$$G_{16_tf}(s) = \frac{-635.4837}{4.735s + 1} e^{-0.415} \quad (20)$$

$$G_{16_least}(s) = \frac{-635.8207}{4.76s + 1} e^{-0.401} \quad (21)$$

In addition, the unit open-loop step responses of $G_{16_tf}(s)$ and $G_{16_least}(s)$ compared to the pitch-speed system $G_{16}(s)$ are shown in Figure 3.

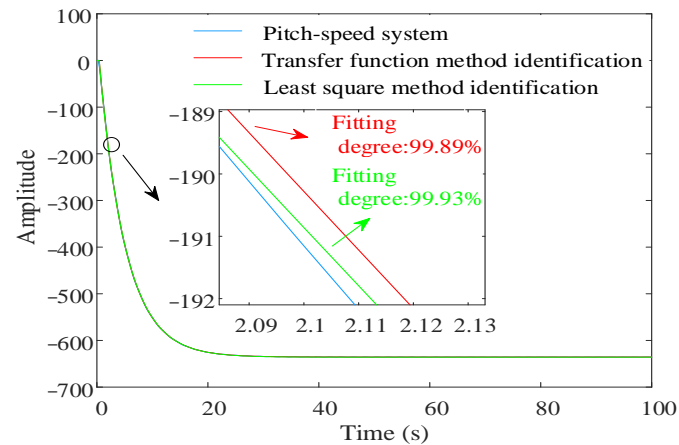


Figure 3. Comparison of unit open-loop step responses.

From the characteristics of the wind turbine, it is clear that the generator speed decreases with increasing pitch angle in the pitch control. Therefore, in Figure 3, the generator speed decreases by 636 r/min when the pitch angle increases by 1 rad.

According to the analysis in Figure 3, the pitch-speed system $G_{16}(s)$ characteristic can be comprehensively reflected by the inertial time-delay system identified by the transfer function and the least squares methods. Moreover, the fitting degree can respectively reach 99.89% and 99.93%. Therefore, $G_{16}(s)$ is identified as $G_{16_least}(s)$ by the least squares method, with higher accuracy.

According to the least squares method, the pitch-speed system for each balance point in 12~25 m/s is identified, in turn.

3.2. Pitch PI Control Parameters Setting

The $G_{16_least}(s)$ is used as the controlled system facilitating the setting of the pitch PI control parameters. Moreover, the Ziegler–Nichols (Z–N) and the Chien–Hrones–Reswick (C–H–R) methods are adopted for setting the pitch PI control parameters.

The slope α needs to be calculated according to the step response being calculated in the Z–N method [24]. The slope α can be expressed as:

$$a = KL/T \quad (22)$$

where K denotes the final value, L denotes the delay, and T denotes the rise time.

The C–H–R method is obtained by improving the Z–N method, allowing larger damping in the controlled system, and directly using T [25]. Therefore, the C–H–R method shows excellent applicability.

According to the Z–N and C–H–R methods, the unit closed-loop step response comparison with both sets of pitch PI control parameters is shown in Figure 4.

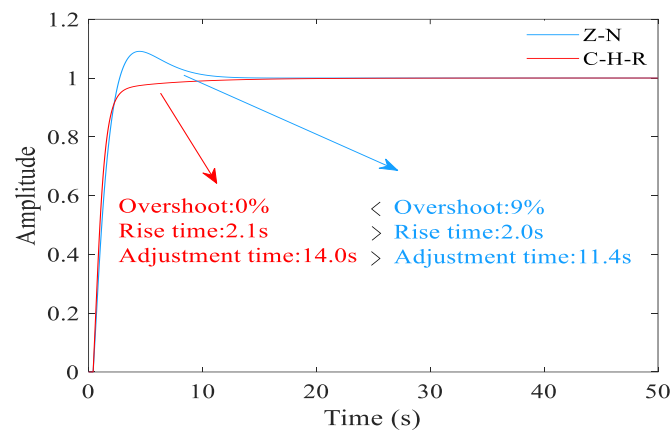


Figure 4. Comparison of unit closed-loop step response.

The unit closed-loop step response amplitude represents a change of output corresponding to when the input changes from 0 to 1. According to the analysis in Figure 4, the control performance for the two sets of pitch PI control parameters satisfies the control requirements. Compared with the C–H–R method, the pitch PI control parameters set using the Z–N method exhibit advantages regarding both rise and adjustment times. Moreover, the overshoot is 9%. The overshoot is the most important measurement index in the unit closed-loop step response. Therefore, a smaller overshoot usually indicates good control performance of pitch PI control parameters. However, the C–H–R method can achieve a 0% overshoot, with similar rise and adjustment times. Therefore, the pitch PI control parameters with better control performance set by the C–H–R method are selected for subsequent optimization, which can be expressed as K_p and K_i .

According to the C–H–R method, pitch PI control parameters for each balance point are set, in turn.

4. Parameter Optimization and Adaptive Control

4.1. Optimization of Control Parameters

Due to the difficulty in accurately setting multiple control parameters in wind turbines, the optimization of the control parameters is essential. Therefore, for enhancing the control performance and reducing the tower vibration and load, the KPGA that can optimize the pitch PI control parameters and the active damping gain for each balance point is proposed.

In general, evolutionary algorithms show excellent robustness benefits. Among these, the GA is extensively adopted due to its broad suitability and excellent optimization performance. In addition, GA can be easily combined with other algorithms for improvement. However, as the wind turbine becomes complex, the need for the improved accuracy of the control parameters also increases. Due to the poor population diversity of GA, falling into the local optimum will lead to an unsatisfactory optimization effect. Therefore, the control parameters based on GA optimization cannot meet the control performance requirements of complex wind turbines.

For solving these problems, the method of KPGA optimization control parameters that can overcome the problem of falling into the local optimum is proposed. Compared with GA, a cross-kindred selection operation is introduced in KPGA. Therefore, the selection operations include both intra-kindred and cross-kindred selection operations. Among these, the intra-kindred selection operation is required for each generation. However, the interval generations selection is adopted in the cross-kindred selection operation to provide enough evolutionary generations for the potential individuals. Therefore, the accidental elimination of excellent potential individuals in the population can be avoided due to crossover and mutation operations, thereby maintaining population diversity and overcoming the problem of falling into the local optimum. In summary, since the KPGA

has excellent global and local search capabilities, high accuracy control parameters can be acquired.

The main parameters are selected as follows [26,27]. The value of population size is selected as 50 to ensure population diversity ($M = 50$). In addition, the parameter settings of the generations need to ensure that the KPGA can achieve stable convergence in the later stages. Therefore, the generations parameter value is selected as 200 ($G = 200$). Moreover, to keep both population diversity and convergence, the crossover and mutation probabilities are selected as 0.9 and 0.1 ($P_c = 0.9$ and $P_m = 0.1$). Furthermore, the value of the cross-kindred selection interval is very important for KPGA. If the cross-kindred selection interval is too small, the KPGA will fall into the local optimum. On the contrary, the algorithm efficiency will be reduced if the cross-kindred selection interval is too large. Therefore, the parameter value of the cross-kindred selection interval is selected as 20 ($T_s = 20$).

According to the above parameters, the flow of the KPGA is shown in Figure 5.

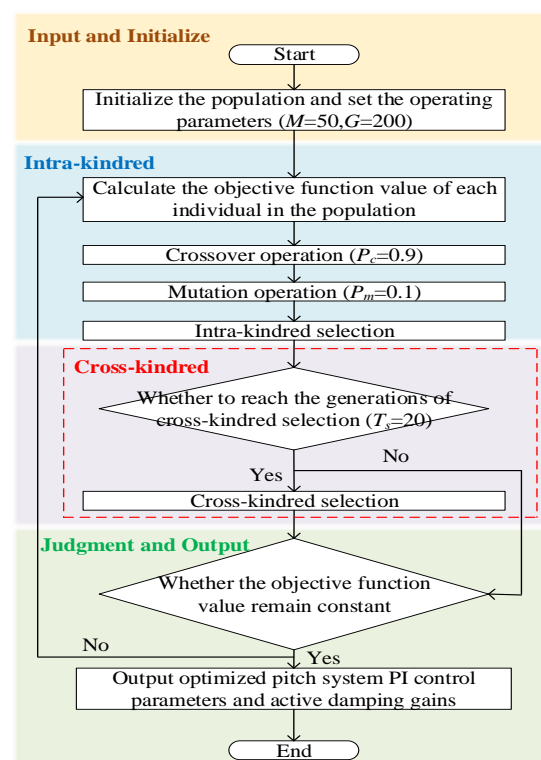


Figure 5. The flow of the KPGA.

Based on the flow of the KPGA, its steps can be summarized in the following five points.

Firstly, the operating parameters of the KPGA are defined. To improve the applicability of the controller for complex wind turbines, the state space equation is selected as the controlled system. Subsequently, turbulent wind types and turbulence intensities are considered as input variables to verify their influence on the optimization results. In order to calculate the objective function value, the generator speed and the fore-aft acceleration of the tower top are set as outputs. Then, the input and output sampling steps are set. Furthermore, optimization is performed with K_p , K_i , and K_a as initial values to obtain higher accuracy control parameters.

Secondly, the objective function F_p can be formed by the generator speed and the tower top fore-aft acceleration, as shown in Equation (23). Then, the objective function values are calculated. Among these, the generator speed Integrated Time and Absolute Error (ITAE) in the objective function can reflect the control performance, and the tower top fore-aft acceleration ITAE can reflect the load situation.

Thirdly, crossover operation, mutation operation, and intra-kindred selection are performed among individuals in the population.

Next, the need for cross-kindred selection is determined based on the cross-kindred selection interval. If necessary, the cross-kindred selection is performed. If not, the cross-kindred selection is skipped, and the next judgment step is performed.

Finally, the optimized pitch PI control parameters and the optimized tower active damping gain are obtained when the objective function value remains constant. Otherwise, the KPGA returns to the second step and re-runs the process.

$$F_p = \zeta \omega_g^{ITAE} + (1 - \zeta) a^{ITAE} \tag{23}$$

where ζ represents the control objective weight, a^{ITAE} represents the tower top fore-aft acceleration ITAE, and ω_g^{ITAE} represents the generator speed ITAE.

Among these, the ITAE is shown in Equation (24).

$$\int_0^\infty t|e(t)|dt \tag{24}$$

where $e(t)$ represents the error function, and t represents time.

Equation (23) is shown in Equations (25) and (26), in detail.

$$\omega_g^{ITAE} = \int_0^\infty (t_{\omega_g} |e_{\omega_g}(t_{\omega_g})|) dt \tag{25}$$

$$a^{ITAE} = \int_0^\infty (t_a |e_a(t_a)|) dt \tag{26}$$

where t_{ω_g} and t_a denote time, and $e_{\omega_g}(t_{\omega_g})$ and $e_a(t_a)$ denote the error function.

In order to coordinate the control performance and load situation, the weight of objective function F_p can be allocated using the Pareto method. Under different turbulent wind speeds and turbulence intensities, the Pareto chart is shown in Figure 6.

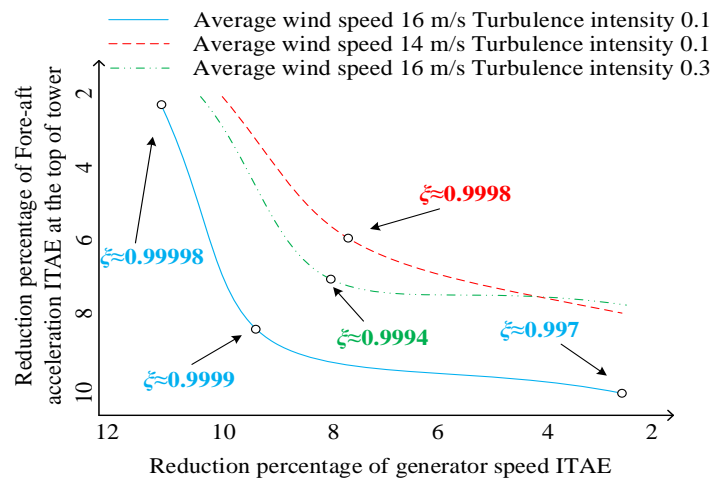


Figure 6. The Pareto chart under different turbulent wind speeds and turbulence intensities.

The generator speed ITAE and tower top fore-aft acceleration ITAE all decrease with the change in ζ under the same wind condition. However, ζ is influenced by turbulence intensities and wind speeds v . The optimal value of ζ is selected on the curve using an eclectic method to enhance the control performance and reduce the load situation. Therefore, the optimal value of ζ under the turbulence intensity of 0.1 and the average wind speed of 16 m/s is 0.9999, based on the Pareto method. As an example, the optimal value of ζ at a turbulence intensity of 0.1 is shown in Equation (27). Using the above method, the equation of the optimal value of ζ for the rest of the turbulent intensities can be obtained.

$$\zeta = 1 - \frac{0.41}{v^3} \tag{27}$$

According to the result of weight allocation, the K_p , K_i , and K_a at a wind speed of 16 m/s can be optimized using the proposed KPGA method. Therefore, the change curve of the objective function values under different wind conditions is shown in Figure 7. In addition, since the objective function value is just a numerical value, it has no units.

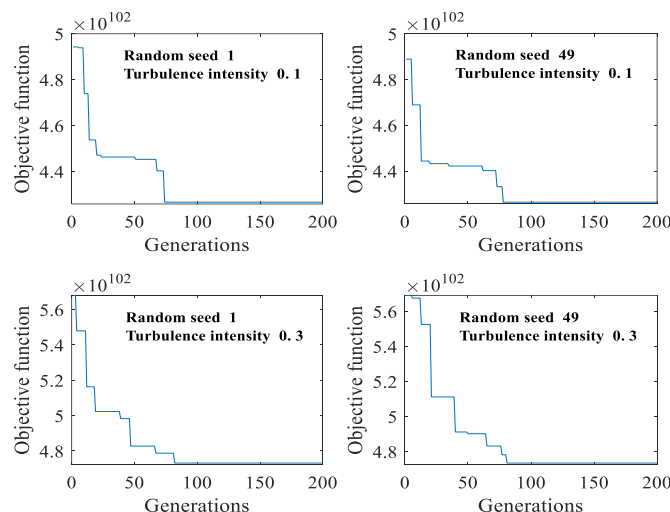


Figure 7. The change curve of the objective function.

It can be observed from Figure 7 that the optimized pitch PI control parameters and active damping gain obtained by KPGA show high accuracy, as the population generations are increasing. Under the same turbulence intensity, the optimization results are hardly influenced by the turbulent wind types, which validates that the proposed KPGA optimization method is highly adaptable for various turbulent wind types. Among these, the random seeds represent the turbulent wind types. The turbulence intensities greatly affect the optimization results at the same turbulent wind type. The optimization of the control parameters is poor due to the wind turbine parameters varying significantly with the wind speed at higher turbulence intensities. Therefore, under the turbulence intensity of 0.1, the proportional coefficient $K_p^{optimal}$, integral coefficient $K_i^{optimal}$, and active damping gain $K_a^{optimal}$ are chosen according to the optimization results at 16 m/s wind speed.

According to the proposed KPGA optimization method, the pitch PI control parameters and active damping gains for each balance point are optimized, in turn.

4.2. Adaptive Control Design

Due to the varying operating states of the wind turbine, the discrete control parameters do not always guarantee excellent control performance when the wind turbine operates away from the balance points [28,29]. Therefore, an adaptive control method is used to enhance the control performance of wind turbines. Specifically, the pitch PI control parameters and active damping gains are fitted with the wind speed points to build the adaptive controller. Therefore, even if the wind turbine operates away from the balance points as the wind conditions vary, the pitch PI control parameters and active damping gains are obtained and updated in real time for a wind speed step of 0.1 m/s using the adaptive controller to ensure an excellent control performance. According to the above analysis, the adaptive control parameters can be designed for each balance point, which is shown in Table 1.

Table 1. The adaptive control parameters designed for each balance point.

Wind Speed (m/s)	12	13	14	...	25
$K_p^{optimal}$	0.030	0.023	0.019	...	0.005
$K_i^{optimal}$	0.012	0.011	0.010	...	0.006
$K_a^{optimal}$	0.195	0.171	0.144	...	0.036

Subsequently, the $K_p^{optimal}$, $K_i^{optimal}$ and $K_a^{optimal}$ for each balance point can be fitted with the wind speed points by using the least squares method. Then, the adaptive control curves are obtained below.

$$K_p^{optimal}(v) = -0.000018v^3 + 0.0012v^2 - 0.027v + 0.21 \tag{28}$$

$$K_i^{optimal}(v) = 0.000002v^3 - 0.0001v^2 + 0.001v + 0.01 \tag{29}$$

$$K_a^{optimal}(v) = 0.001v^2 - 0.05v + 0.65 \tag{30}$$

where $K_p^{optimal}(v)$ and $K_i^{optimal}(v)$ represent the adaptive control curve of the pitch PI control, and $K_a^{optimal}(v)$ represents the adaptive control curve of the active damping control.

The fitting accuracy of the above equations is 97.56%, 98.35%, and 99.14%, which satisfies the practical engineering standard. Thereby, the adaptive control method can obtain and update the control parameters with a wind speed step of 0.1 m/s. The adaptive control curve is shown below.

In Figure 8, it can be observed that the accurate control parameters can still be obtained with wind speed steps of 0.1 m/s by the adaptive controller when the wind turbine operates away from the balance points. Therefore, the adaptive controller can maintain a better control performance.

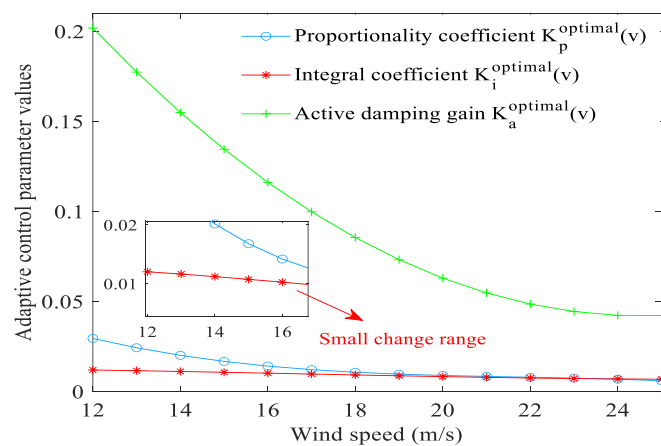


Figure 8. The designed for adaptive control.

5. Simulations

The simulation models are as follows: Mode 1: The adaptive pitch PI control with unoptimized (PI). Mode 2: The adaptive pitch PI control and adaptive tower fore-aft active damping control with unoptimized (PI + D). Mode 3: The adaptive pitch PI control and adaptive tower fore-aft active damping control with GA optimized (PI + D + GA). Mode 4: The adaptive pitch PI control and adaptive tower fore-aft active damping control with KPGA optimized (PI + D + KPGA). By comparing Modes 1 and 2, the effect of the tower active damping control method can be verified. By comparing Modes 2 and 3, the effect of the GA control parameter optimization method can be verified. By comparing Modes 3 and 4, the effect of the KPGA compared to the control parameter optimization method can be verified.

5.1. Frequency Domain Simulations

The pitch system Bode plot is shown in Figure 9, which can verify the pitch system stability. The Bode plot reflects the frequency response when wind speed is used as an input. The output of the Bode plot represents the generator speed. The Bode plot represents the relationship between the ratio of output and input.

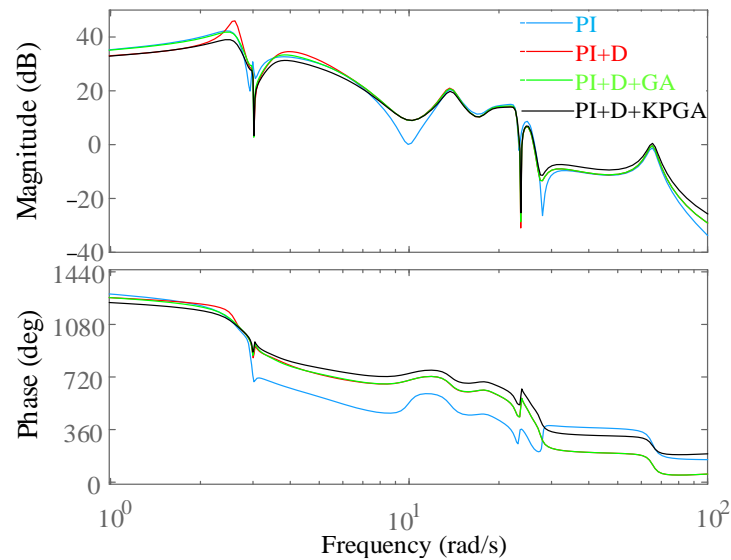


Figure 9. The pitch system Bode plot.

In comparing Modes 1 and 2, the phase and magnitude margins are above 0, indicating a sufficient stability margin for the pitch system.

In comparing Modes 2 and 3, according to the optimized GA, the pitch system shows a sufficient stability margin.

In comparing Modes 3 and 4, by optimizing the control parameters based on KPGA, the pitch system can maintain stability.

The active damping control Bode plot reflects the response of the tower top fore-aft velocity to the wind speed, which is shown in Figure 10. The active damping control Bode plot reflects the frequency response when wind speed is used as an input. The output of the active damping control Bode plot represents the tower top fore-aft velocity.

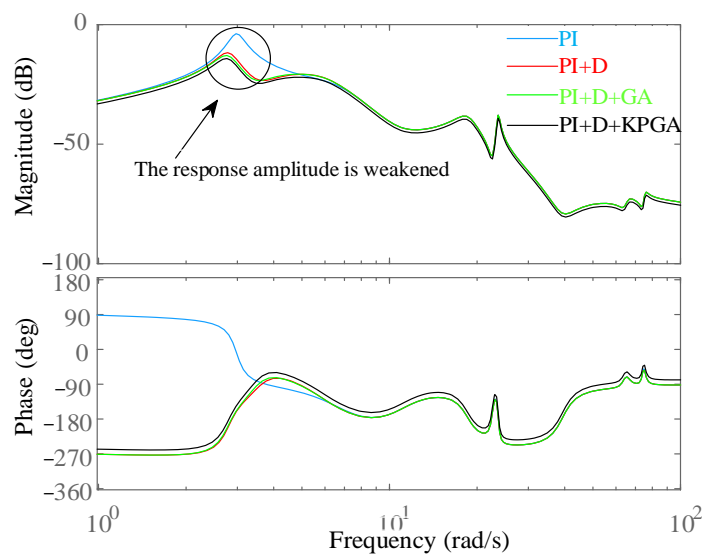


Figure 10. The active damping control Bode plot.

In comparing Modes 1 and 2, the response magnitude of the tower top fore-aft velocity to the wind speed is significantly weakened near 2.95 rad/s. The first-order modal natural frequency fore-aft of the tower is 2.95 rad/s. Therefore, the first-order modal natural damping of the tower is increased by active damping control, thereby significantly restraining the fore-aft vibrations of the tower top.

In comparing Modes 2 and 3, the active damping control of the tower always maintain stability. Moreover, control parameters with optimized GA can further restrain the fore-aft vibrations of the tower top.

In comparing Modes 3 and 4, it can be observed that the optimization of the control parameters based on KPGA can further restrain fore-aft vibration, compared to GA.

The self-power spectral density can reflect the tower top fore-aft acceleration per unit frequency. Therefore, the self-power spectral density of the fore-aft acceleration for the tower top is shown in Figure 11.

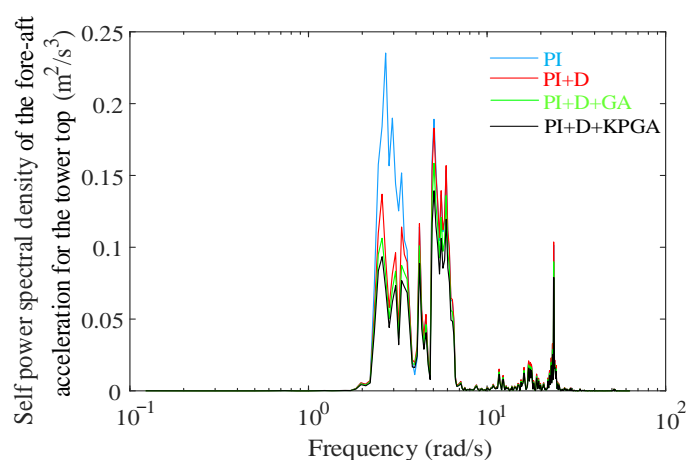


Figure 11. Self-power spectral density of the fore-aft acceleration for the tower top.

In comparing Modes 1 and 2, the self-power spectral density of the fore-aft acceleration for the tower top is remarkably reduced near 2.95 rad/s. Thus, the tower top resonance is restrained.

In comparing Modes 2 and 3, the self-power spectral density is further reduced near 2.95 rad/s. Therefore, the tower top fore-aft vibration is further restrained by optimizing the control parameters based on GA.

In comparing Modes 3 and 4, the optimized control parameters based on KPGA can further reduce the self-power spectral density near 2.95 rad/s, compared to GA.

5.2. Time Domain Simulations

The design load cases (DLCs) are designed according to the GL 2003 standard. The representative simulation results of power production DLC1.1 are selected for presentation.

The wind turbine operates in the pitch control range when the turbulent wind is 16 m/s. It can be defined as shown in Figure 12. Therefore, the parameter settings of the simulation environment can meet the standard requirements.

The pitch angle can reflect the control effect of the active damping control. Therefore, the change curve of the pitch angle under the wind speed of 16 m/s is shown below.

By analyzing Figure 13, the additional pitch angle can be provided in Modes 2, 3, and 4. Therefore, the tower active damping control plays an important role in pitch control. Compared to the methods used in references [16,18], the proposed design method has an excellent control performance for the pitch angle, which can reduce the fluctuations in the pitch angle.

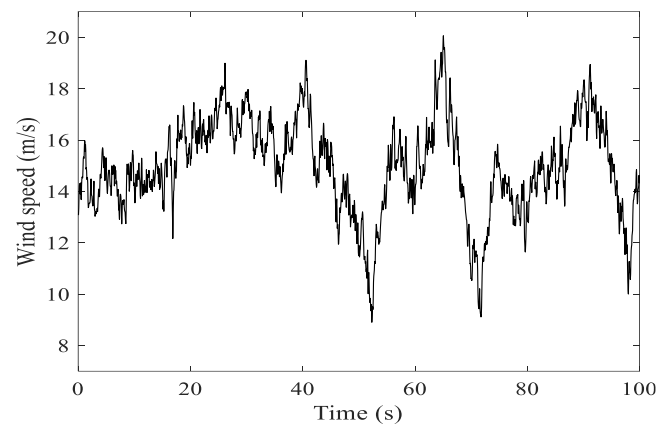


Figure 12. Turbulent wind of 16 m/s.

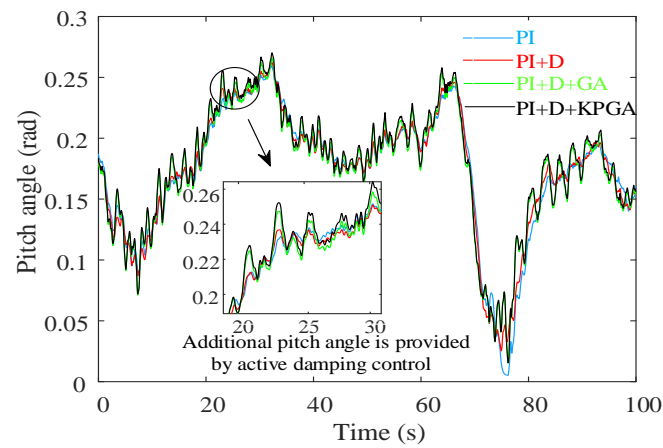


Figure 13. Change curve of the pitch angle.

(1) The control performance.

The control performance can be reflected by the change curves of output power and generator speed. Therefore, they are shown in Figures 14 and 15.

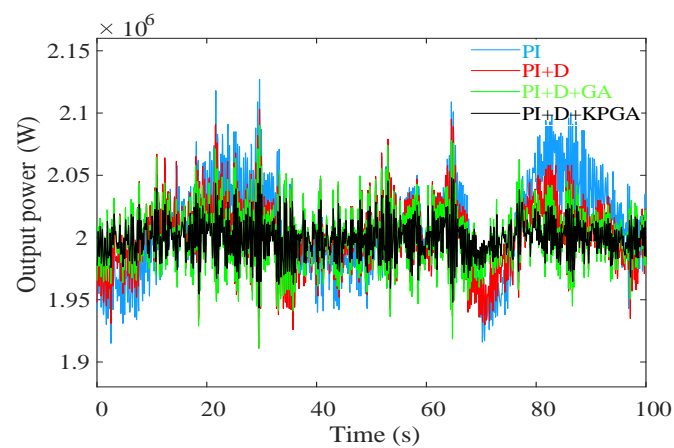


Figure 14. Change curve of output power.

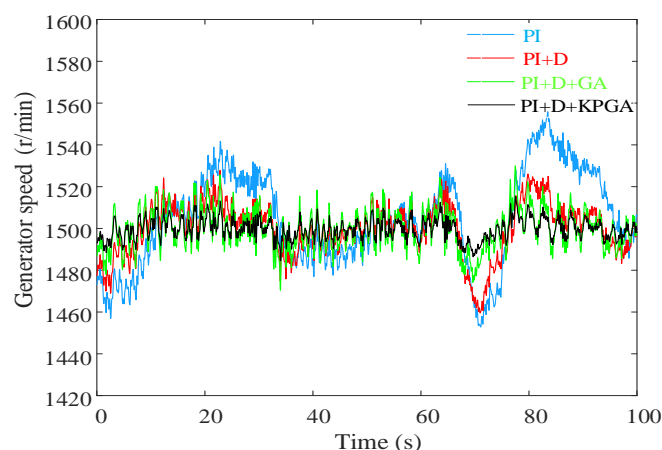


Figure 15. Change curve of generator speed.

The analysis Figures 14 and 15 is shown in Table 2.

Table 2. The control performance indicators.

	Mode 1	Mode 2	Mode 3	Mode 4
Output power MEAN (W)	1.999×10^6	2.000×10^6	2.000×10^6	2.000×10^6
Output power RMSE	3.648×10^4	3.484×10^4	2.628×10^4	2.536×10^4
Generator speed MEAN (r/min)	1.506×10^3	1.503×10^3	1.501×10^3	1.500×10^3
Generator speed RMSE	2.241×10^1	1.885×10^1	1.362×10^1	1.248×10^1

In comparing Modes 1 and 2, the output power MEAN is increased by 1 kW. Its RMSE is reduced by 4.50%. Furthermore, generator speed MEAN and RMSE are reduced by 0.20% and 15.89%, respectively.

In comparing Modes 2 and 3, the output power MEAN is ensured at the rated output power. Its RMSE is reduced by 24.57%. Furthermore, the generator speed MEAN and RMSE are reduced by 0.13% and 27.75%, respectively.

In comparing Modes 3 and 4, the output power MEAN is ensured at the rated output power. Its RMSE is reduced by 3.50%. Furthermore, the generator speed MEAN and RMSE are reduced by 0.07% and 8.37%, respectively.

Compared to the methods used in references [14,16], the proposed design method can significantly reduce the fluctuations of output power and generator speed.

(2) The tower fore-aft vibration.

The tower fore-aft vibration can be reflected by the change curves of the fore-aft acceleration and velocity of the tower top. Therefore, they are shown in Figures 16 and 17.

The analysis of Figures 16 and 17 is shown in Table 3.

In comparing Modes 1 and 2, the tower top fore-aft acceleration RANGE and MEAN are reduced by 35.13% and 43.12%, respectively. Furthermore, the tower top fore-aft velocity RANGE and MEAN are reduced by 45.79% and 56.80%, respectively.

In comparing Modes 2 and 3, the tower top fore-aft acceleration RANGE and MEAN are reduced by 32.04% and 28.43%, respectively. Furthermore, the tower top fore-aft velocity RANGE and MEAN are reduced by 20.39% and 27.95%, respectively.

In comparing Modes 3 and 4, the tower top fore-aft acceleration RANGE and MEAN are reduced by 20.33% and 19.18%, respectively. Furthermore, the tower top fore-aft velocity RANGE and MEAN are reduced by 9.76% and 11.48%, respectively.

Compared with the method used in reference [9], the proposed design method can significantly reduce the tower top fore-aft vibration.

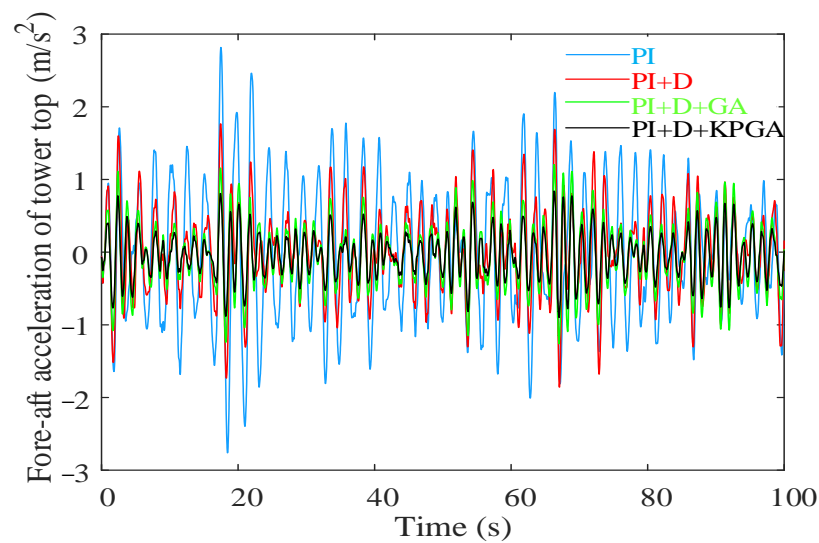


Figure 16. Change curve of fore-aft acceleration for the tower top.

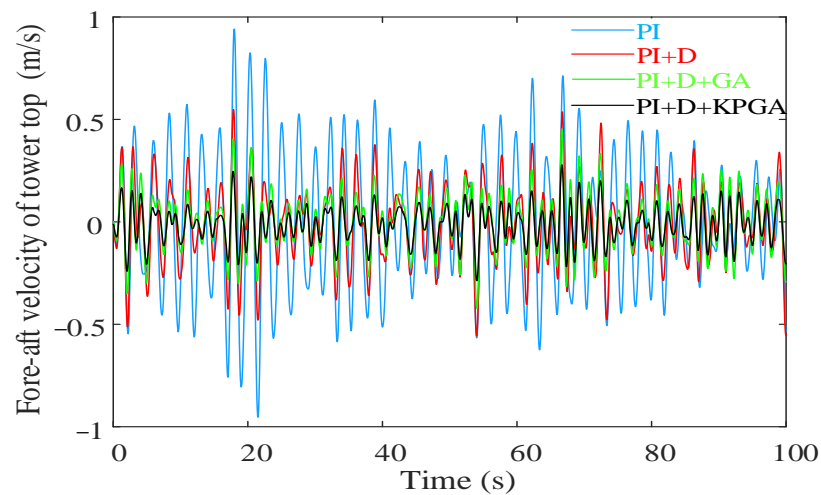


Figure 17. Change curve of fore-aft velocity for the tower top.

Table 3. The tower fore-aft vibration indicators.

	Mode 1	Mode 2	Mode 3	Mode 4
Acceleration RANGE (m/s ²)	0.558×10^1	0.362×10^1	0.246×10^1	0.196×10^1
Acceleration MEAN (m/s ²)	-0.538×10^{-2}	-0.306×10^{-2}	-0.219×10^{-2}	-0.177×10^{-2}
Velocity RANGE (m/s)	0.190×10^1	0.103×10^1	0.082×10^0	0.074×10^0
Velocity MEAN (m/s)	0.588×10^{-4}	0.254×10^{-4}	0.183×10^{-4}	0.162×10^{-4}

(3) The tower x-direction load.

The tower x-direction load can be reflected by the change curves of the x-direction torque and force of the tower bottom. Therefore, the timing sequence load is shown in Figures 18 and 19.

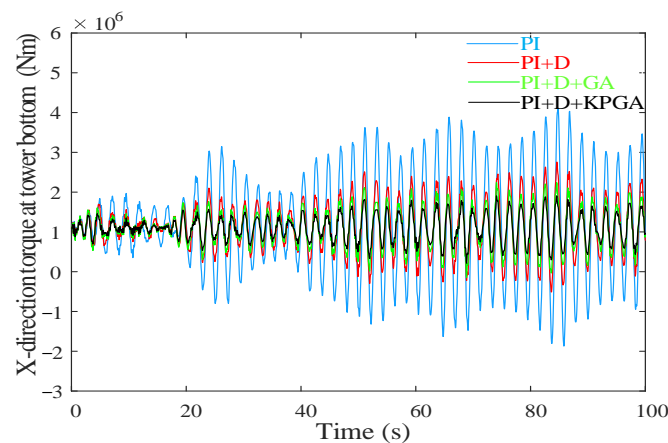


Figure 18. Change curve of x-direction torque for the tower bottom.

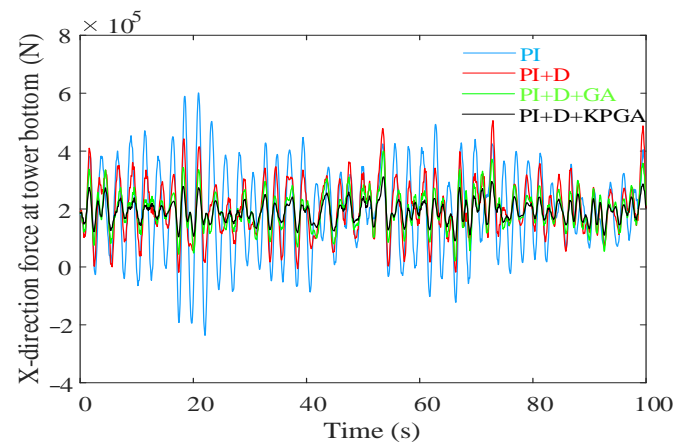


Figure 19. Change curve of x-direction force for the tower bottom.

The analysis of Figures 18 and 19 is shown in Table 4.

Table 4. The tower x-direction load indicators.

	Mode 1	Mode 2	Mode 3	Mode 4
Mx RANGE (Nm)	5.962×10^6	2.893×10^6	1.915×10^6	1.479×10^6
Mx MEAN (Nm)	1.157×10^6	1.153×10^6	1.151×10^6	1.150×10^6
Fx RANGE (N)	6.384×10^5	4.542×10^5	3.823×10^5	3.451×10^5
Fx MEAN (N)	1.938×10^5	1.933×10^5	1.930×10^5	1.928×10^5

The damage equivalent load (DEL) is calculated by the timing sequence load of the x-direction torque and the force of the tower bottom, which is shown in Table 5.

Table 5. The DEL indicators.

	Mode 1	Mode 2	Mode 3	Mode 4
Mx DEL (Nm)	9.96×10^6	9.74×10^6	9.68×10^6	9.64×10^6
Fx DEL (N)	5.99×10^5	5.89×10^5	5.86×10^5	5.84×10^5

In comparing Modes 1 and 2, the tower bottom Mx RANGE and MEAN are reduced by 51.48% and 0.35%, respectively. Furthermore, the tower bottom Fx RANGE and MEAN are reduced by 28.85% and 0.26%, respectively. Besides, the tower bottom Mx and Fx DEL are reduced by 2.21% and 1.67%, respectively.

In comparing Modes 2 and 3, the tower bottom Mx RANGE and MEAN are reduced by 33.81% and 0.17%, respectively. Furthermore, the tower bottom Fx RANGE and MEAN are reduced by 15.83% and 0.16%, respectively. Besides, the tower bottom Mx and Fx DEL are reduced of 0.62% and 0.51%, respectively.

In comparing Modes 3 and 4, the tower bottom Mx RANGE and MEAN are reduced by 22.77% and 0.09%, respectively. Furthermore, the tower bottom Fx RANGE and MEAN are reduced by 9.73% and 0.10%, respectively. Besides, the tower bottom Mx and Fx DEL are reduced by 0.41% and 0.34%, respectively.

Compared with the method used in reference [6], the proposed design method can significantly reduce the tower bottom load.

6. Conclusions

Given the difficulty in accurately setting multiple control parameters in wind turbines, the design method for a pitch controller considering tower load reduction is proposed, which enhances the control performance and reduces the tower vibration and load. The conclusions are shown below.

- (1) In regards to the frequency domain simulations, the pitch system is sufficiently stable. Near 2.95 rad/s, the response amplitude of the tower top fore-aft velocity to the wind speed can be weakened. Moreover, the self-power spectral density of the fore-aft acceleration for the tower top can be significantly reduced near 2.95 rad/s.
- (2) For the time domain simulations, the control performance can be enhanced. In addition, the tower top fore-aft vibration can be restrained, and the tower bottom x-direction load can be reduced.

In the future, torque control strategies for increasing power generation will become a research hotspot. In addition, methods for reducing drive chain load have been widely studied in recent years. Therefore, the above method is a promising focus for future research.

Author Contributions: Conceptualization, Y.L. and S.Z.; methodology, X.W. and H.X.; software, S.Z.; validation, S.Z. and T.C.; formal analysis, Y.L. and S.Z.; resources, Y.L.; writing—original draft preparation, S.Z.; writing—review and editing, S.Z. and T.C.; funding acquisition, Y.L. All authors have read and agreed to the published version of the manuscript.

Funding: This research was funded by the National Natural Science Foundation of China (No. 52007124) and Liaoning Province Central Leading Local Science and Technology Development Funds Program Project (2021JH6/10500166) and The unveiling of the list of hanging science and technology research and development special (2021JH1/10400009).

Data Availability Statement: The data that support the research of this paper are available upon reasonable request from the corresponding author and with the permission of the Shenyang University of Technology.

Acknowledgments: The authors would like to thank Shenyang Huaren Wind Power Technology Co., Ltd. for providing the 2MW wind turbine data and test platform.

Conflicts of Interest: The authors declare no conflict of interest.

Appendix A

Equation (2) can be specifically expressed as follows.

A is a $45 \times 45 \times 22$ matrix. The upper left 7×3 corner of the matrix for the first balance point can be represented as:

$$A = \begin{bmatrix} 0 & 0 & 0 \\ -0.0001 \times 10^5 & 0 & 0 \\ 0 & 0 & 0 \\ 0 & 0 & -0.0001 \times 10^5 \\ 0 & 0 & 0 \\ 0 & 0 & 0 \\ 0 & 0 & 0 \end{bmatrix} \quad (\text{A1})$$

B is a $45 \times 3 \times 22$ matrix. The upper left 7×3 corner of the matrix for the first balance point can be represented as:

$$B = \begin{bmatrix} 0 & 0 & 0 \\ 0 & -0.0003 & 0 \\ 0 & 0 & 0 \\ 0.0162 & 0.0002 & 0 \\ 0 & 0 & 0 \\ 0 & 0 & 0 \\ 0 & 0 & 0 \end{bmatrix} \quad (\text{A2})$$

C is a $12 \times 45 \times 22$ matrix. The upper left 7×3 corner of the matrix for the first balance point can be represented as:

$$C = \begin{bmatrix} 0 & 0 & 0 \\ 0 & 0 & 0 \\ 0 & 0 & 0 \\ 0 & 0 & 0 \\ 0 & 0 & 0 \\ 0 & 0 & 0 \\ -0.0865 \times 10^9 & -0.0003 \times 10^9 & 0 \end{bmatrix} \quad (\text{A3})$$

D is a $12 \times 3 \times 22$ matrix. The upper left 7×3 corner of the matrix for the first balance point can be represented as:

$$D = \begin{bmatrix} 0 & 0 & 0.846 \times 10^3 \\ 0 & 0 & 0 \\ 0 & 0 & 0.001 \times 10^3 \\ 0 & 0 & 0 \\ 0 & 0 & 0 \\ 0 & 0 & 0 \\ -0.0137 \times 10^3 & -0.1039 \times 10^3 & -0.0010 \times 10^3 \end{bmatrix} \quad (\text{A4})$$

x includes 45 state variables. The first three are shown below.

Table A1. Partial state variables.

	State Variables
1	Tower displacement Mode 1
2	Tower velocity Mode 1
3	Tower acceleration mode 1

u includes 3 input variables.

Table A2. Input variables.

	Input Variables
1	Wind speed
2	Pitch angle demand
3	Generator torque demand

y includes 12 output variables.

Table A3. Output variables.

	Output Variables
1	Measured power
2	Measured generator speed
3	Generator torque
4	Pitch angle
5	Tower M _x , Height = −15 m
6	Tower F _x , Height = −15 m
7	Tower M _y , Height = −15 m
8	Tower F _y , Height = −15 m
9	Tower fore-aft acceleration, height = 60 m
10	Tower fore-aft velocity, height = 60 m
11	Tower side-side acceleration, height = 60 m
12	Tower side-side velocity, height = 60 m

References

- Chojaa, H.; Derouich, A.; Taoussi, M.; Chehaidia, S.E.; Zamzoum, O.; Mosaad, M.I.; Alhejji, A.; Yessef, M. Nonlinear Control Strategies for Enhancing the Performance of DFIG-Based WECS under a Real Wind Profile. *Energies* **2022**, *15*, 6650. [\[CrossRef\]](#)
- Abo-Khalil, A.G.; Alyami, S.; Sayed, K.; Alhejji, A. Dynamic Modeling of Wind Turbines Based on Estimated Wind Speed under Turbulent Conditions. *Energies* **2019**, *12*, 1907. [\[CrossRef\]](#)
- Rosado, L.; Samanes, J.; Gubía, E.; López, J. Robust Active Damping Strategy for DFIG Wind Turbines. *IEEE Trans. Power Electron.* **2021**, *36*, 14525–14538. [\[CrossRef\]](#)
- Dong, H.; Edrah, M.; Zhao, X.; Collu, M.; Xu, X.; Abhinav, K.A.; Lin, Z. Model-Free Semi-Active Structural Control of Floating Wind Turbines. In Proceedings of the 2020 Chinese Automation Congress (CAC), Shanghai, China, 6–8 November 2020; pp. 4216–4220.
- Mukoni, E.; Garner, K.S. Multi-Objective Non-Dominated Sorting Genetic Algorithm Optimization for Optimal Hybrid (Wind and Grid)-Hydrogen Energy System Modelling. *Energies* **2022**, *15*, 7079. [\[CrossRef\]](#)
- Xu, B.; Yuan, Y.; Liu, H.; Jiang, P.; Gao, Z.; Shen, X.; Cai, X. A Pitch Angle Controller Based on Novel Fuzzy-PI Control for Wind Turbine Load Reduction. *Energies* **2020**, *13*, 6086. [\[CrossRef\]](#)
- Xie, X.; Li, H.; Xia, G.; Yao, R.; Chai, Z.; Liu, X. Improved Parameter Identification and Control Strategy of Pitch Motor in Wind Turbine System. In Proceedings of the 2019 IEEE International Symposium on Predictive Control of Electrical Drives and Power Electronics (PRECEDE), Quanzhou, China, 31 May 2019–2 June 2019; pp. 1–6.
- Sundari, K.T.; Komathi, C.; Durgadevi, S.; Abirami, K. Optimal Controller tuning of a PI controller for a three tank non-interacting process. In Proceedings of the 2020 International Conference on Power, Energy, Control and Transmission Systems (ICPECTS), Chennai, India, 10–11 December 2020; pp. 1–5.
- Lio, W.H.; Jones, B.L.; Rossiter, J.A. Estimation and Control of Wind Turbine Tower Vibrations Based on Individual Blade-Pitch Strategies. *IEEE Trans. Control. Syst. Technol.* **2019**, *27*, 1820–1828. [\[CrossRef\]](#)
- Turksoy, O.; Ayasun, S.; Hames, Y.; Sönmez, Ş. Computation of Robust PI-Based Pitch Controller Parameters for Large Wind Turbines. *Can. J. Electr. Comput. Eng.* **2019**, *43*, 57–63. [\[CrossRef\]](#)
- Wang, S.; Liang, H.; Wang, J. GA PID control research in inverter motor speed governing system. *J. Comput. Methods Sci. Eng.* **2018**, *19*, 299–306. [\[CrossRef\]](#)
- Long, Z.; Jiang, Z.; Wang, C.; Jin, Y.; Cao, Z.; Li, Y. A Novel Approach to Control of Piezo-Transducer in Microelectronics Packaging: PSO-PID and Editing Trajectory Optimization. *IEEE Trans. Compon.* **2020**, *10*, 795–805. [\[CrossRef\]](#)
- Al-Kaabi, M.; Dumbrava, V.; Eremia, M. A Slime Mould Algorithm Programming for Solving Single and Multi-Objective Optimal Power Flow Problems with Pareto Front Approach: A Case Study of the Iraqi Super Grid High Voltage. *Energies* **2022**, *15*, 7473. [\[CrossRef\]](#)
- Gao, F.; Ling, X.; Wang, W. PI Parameters Joint Tuning for Individual Pitch Controller of Large Wind Turbine. *Acta Energ. Sol. Sin.* **2018**, *39*, 307–314.
- Song, Z.; Liu, J.; Hu, Y.; Cheng, Y.; Tan, F. Real-Time Performance Analyses and Optimal Gain-Scheduling Control of Offshore Wind Turbine Under Ice Creep Loads. *IEEE Access.* **2019**, *7*, 181706–181720. [\[CrossRef\]](#)

16. Tian, D.; Gao, Y.; Yan, X.M.; Deng, Y. Optimization of Pitch Controller Parameters for Wind Turbine Based on Differential Evolution Algorithm. *Acta Energ. Sol. Sin.* **2019**, *40*, 2154–2161.
17. Ye, H. *Wind Turbine Monitoring and Control*, 2nd ed.; China Machine Press: Beijing, China, 2018; pp. 77–114.
18. Iqbal, A.; Deng, Y.; Saleem, A.; Hayat, M.A.; Mateen, M. Proposed particle swarm optimization technique for the wind turbine control system. *Meas. Control.* **2020**, *53*, 1022–1030. [[CrossRef](#)]
19. Ye, H. *Wind Turbine Control Technology*, 3rd ed.; China Machine Press: Beijing, China, 2015; pp. 143–157.
20. Ying, Y.; Zhu, C.; Yang, F.; Xu, G.D. Development of Active Tower Damping Control on Wind Turbines. *Acta Energy. Sol. Sin.* **2015**, *36*, 54–60.
21. Cao, Q. Seismic Performance Analysis and Safety Assessment of Wind Turbine Tower System. In Proceedings of the 2021 7th International Conference on Hydraulic and Civil Engineering & Smart Water Conservancy and Intelligent Disaster Reduction Forum (ICHCE & SWIDR), Nanjing, China, 6–8 November 2021; pp. 1024–1030.
22. Xue, D. *Computer Aided Control Systems Design Using MATLAB Language*, 3rd ed.; Tsinghua University Press: Beijing, China, 2012; pp. 318–321.
23. Ji, Y.; Lv, L. M-Decomposed Least Squares and Recursive Least Squares Identification Algorithms for Large-Scale Systems. *IEEE Access.* **2021**, *9*, 139466–139472. [[CrossRef](#)]
24. Ling, Y. Effect Analysis of Z-N Method Combined with GA on PID Parameter Optimization of Screw Extruder. In Proceedings of the 2022 IEEE 6th Information Technology and Mechatronics Engineering Conference (ITOEC), Chongqing, China, 4–6 March 2022; pp. 1548–1551.
25. Gao, F.; Wang, W. Parameters Tuning and Optimization of Variable-gain PI Controller of Wind Turbine Based on Immune Genetic Algorithm. *J. Chin. Soc. Power Eng.* **2016**, *36*, 22–29.
26. Wei, H.; Li, S.; Quan, H.; Liu, D.; Rao, S.; Li, C.; Hu, J. Unified Multi-Objective Genetic Algorithm for Energy Efficient Job Shop Scheduling. *IEEE Access.* **2021**, *9*, 54542–54557. [[CrossRef](#)]
27. Chen, G.; Gou, X.; Zhang, J. Voltage stability Hopf bifurcation control based on two-stage family protection genetic algorithm. *Power Syst. Technol.* **2021**, *35*, 53–58.
28. Puchta, E.D.P.P.; Siqueira, H.V.; Kaster, M.d.S. Optimization Tools Based on Metaheuristics for Performance Enhancement in a Gaussian Adaptive PID Controller. *IEEE Trans. Cybern.* **2020**, *50*, 1185–1194. [[CrossRef](#)]
29. Sun, Y.; Xu, J.; Chen, C.; Hu, W. Reinforcement Learning-Based Optimal Tracking Control for Levitation System of Maglev Vehicle with Input Time Delay. *IEEE Trans. Instrum. Meas.* **2022**, *71*, 1–13. [[CrossRef](#)]